Supplement of

Aging impact on sources, volatility, and viscosity of organic aerosols in the Chinese outflows

Feng et al.

Correspondence: Weiwei Hu (weiweihu@gig.ac.cn)

1 Experiment

1.1 PMF and ME-2 analysis

The initial high-resolution OA data and error matrix ranging from m/z 12 to m/z 120 were put into the PMF analysis of this study, while the isotope ions and ions with the low signal-to-noise ratio (SNR < 0.2) were removed. Ions with weak SNR (0.2 < SNR < 2) and CO_2^+ related ions (CO_2^+, CO^+, H_2O^+, HO^+, O^+) were downweighed by increasing the error with a factor of 2.23 (Zhang et al., 2011; Ulbrich et al., 2009)

At first, unconstrained source apportionment was conducted (Seed=1=10 or Fpeak 0-1) based on PMF Evaluation Tool (PET, version 2.08) (Ulbrich et al., 2009). As the Q/Q_{exp} decreases, no biomass burning factor was resolved in 3-4 factor solutions. However, biomass burning was indeed seen during the campaign. Biomass burning-related factor was resolved when 5-7 factors were chosen whereas this solution was not the best due to splitting OOA factors. Thus, ME-2 was applied here. Both HOA and BBOA were constrained in ambient only and ambient combined TD datasets using SoFi v6.81 with different α values from 0 to 1, where a value represents the constrained extent in the standard mass spectral profile (0 means strictly constrained, 1 means unconstrainted) (Zhang et al., 2011; Huang et al., 2014; Canonaco et al., 2013). As shown in Fig. S3, an obvious difference was found between time series from ambient and ambient combined TD datasets when 4 factors were chosen with a value=0, thus 4 factors with HOA and BBOA being constrained in ME2 here is not the best solution here. When 5 factors were chosen, a splitting of the HOA time series was found. The constrained HOA is very noisy and shows very low contributions to total OA (< 4 %). Meanwhile, the constrained HOA factor exhibits a very similar variation to the aged-HOA here (R=0.52), as shown in Fig. S4. Thus, we do not think the 5-factor solution with both HOA and BBOA being constrained is good as well. Instead, we only constrain BBOA without constraining HOA, since the aged-HOA can be resolved without being constrained. Here, the strong BBOA spectrum was obtained from Changdao campaign, which was conducted in a similar season and nearby location to Dongying study (Hu et al., 2013). Finally, the most environmentally meaningful solution of 4 factors with BBOA being constrained (a value=0) was chosen for the final solution. The correlations of four factors, namely BBOA, aged-HOA, transported-OOA, and background-OOA, with external tracers can be found in Fig. S5.

To investigate the volatilities of different OA factors, ME-2 analysis was also applied to the OA matrix combined with ambient and TD measurements. As shown in Fig. S6, there is a good correlation between the ambient dataset and ambient + TD datasets.

1.2 Calibrations of transmission and temperature of TD

We used the formula proposed by Huffman et al. (2008) to calibrate the transmission and temperature of TD since their residence times are similar (about 21s).

$$\text{TD Transmission} = -0.00082 * \text{Temp}_{\text{centerline, real}} + 0.98 \quad (1)$$

Where TD transmission represents the aerosol mass ratio between TD and ambient lines due to particle loss. $\text{Temp}_{\text{centerline, real}}$ is the real centerline temperature, which was found to be about 17 % higher than the set temperature controlled by TD software ($\text{Temp}_{\text{TD-set}}$). The centerline temperature can be corrected with the following eq. (2):

$$\text{Temp}_{\text{centerline, real}} = 1.1732 * \text{Temp}_{\text{TD-set}} - 7.7625 \quad (2)$$

To compare the thermograms from different experiments with similar TD setup, each mass thermogram was fitted by the Hill's Equation, a type of sigmoidal function, to obtain the T_{50} value, which is the temperature at which MFR = 0.50 (Kolesar et al., 2015; Emanuelsson et al., 2013).

$$MFR(T) = MFR_{max} + \left(\frac{MFR_{min} - MFR_{max}}{1 + \left(\frac{T_{50}}{T}\right)^{S_{MFR}}}\right) \quad (3)$$

where MFR_{min} and MFR_{max} are the MFR values at the highest and lowest temperatures, S_{MFR} is the slope representing the steepness of the curve of MFR.

1.3 Predictions of glass transition temperature and viscosity of organic aerosols

The glass transition temperature (T_g) represents the temperature where phase transition occurs between semisolid and glassy states. T_g of organic aerosols can be estimated based on the volatility distributions, as shown in Eq. (4):

$$T_{g,i} = 289.10 - 16.5 \times \log_{10}\left(C_i^0\right) - 0.29 \times \left[\log_{10}\left(C_i^0\right)\right]^2 + 3.23 \times \log_{10}\left(C_i^0\right) \times (O{:}C) \quad (4)$$

where C_i^0 is saturation vapor pressure (C^*, unit: μg m^{-3}) at 298 K and O:C is determined by the A-A method (Unit: dimensionless). Then the T_g of organic aerosols ($T_{g,org}$) under dry conditions can be calculated by a simplified Gordon–Taylor equation assuming the Gordon–Taylor constant (k_{GT}) =1 as shown in Eq. (5), where ω_i is the fraction of particulate organic aerosols per volatility bin (Dette et al., 2014).

$$T_{g,org} = \sum_i \omega_i T_{g,i} \quad (5)$$

In addition, Gordon–Taylor equation is also used to calculate T_g of organic-water ($T_{g,\omega org}$) mixture at a given RH by assuming k_{GT}=2.5.

$$T_{g,\omega_{org}} = \frac{(1-\omega_{org})T_{g,w} + \frac{1}{k_{GT}}\omega_{org}T_{g,org}}{(1-\omega_{org}) + \frac{1}{k_{GT}}\omega_{org}} \quad (6)$$

$T_{g,w}$ represents the glass transition temperature of the water, generally 136 K (Koop et al., 2011). ω_{org} ($\omega_{org}=m_{OA}/m_{OA}+m_{H2O}$) is the mass fraction of organic species (m_{OA}) and water (m_{H2O}) in the particle phase. The total mass concentration of water can be determined by effective hygroscopicity parameters of organics κ_{org} (κ_{org}= 2.10 (± 0.07) × f_{44} − 0.11 (± 0.01)), where f_{44} is the fraction of m/z 44 signal in total organic signals (Mei et al., 2013).

$$m_{H2O} = \frac{\kappa_{org}\rho_w m_{org}}{\rho_{org}(\frac{1}{a_w}-1)} \quad (7)$$

The density of organic aerosols (ρ_{org}) and the water (ρ_w) in this study were estimated to be 1.44 g cm^{-3} (Kuwata et al., 2012) and 1g cm^{-3}, respectively. a_w represents water activity, which is calculated by a_w = RH/100.

Then we can calculate temperature-dependent viscosity (η) by the modified Vogel-Tammann-Fulcher (VTF) equation (Eq. (8)).

$$\eta = \eta_\infty e^{\frac{T_0 D}{T-T_0}} \quad (8)$$

where η_∞ =10^{-5} Pa s, $T_0 = \frac{39.17\, T_{g,\omega org}}{D+39.17}$. D is the fragility parameter usually assumed to be 10 (Derieux et al., 2018).

The timescale of particle diffusion is characterized by mixing time (τ_{mix}) according to Eq. (9), where d_p is the particle diameter (d_p of ambient OA is about 550 nm, which is assumed 200 nm here for comparison with other studies conveniently (Xu et al., 2021; Li et al., 2020; Evoy et al., 2019)), and the bulk diffusion coefficient D_b is calculated from the predicted viscosity by the fractional Stokes-Einstein relation, as shown in Eq. (10) (Xu et al., 2021; Evoy et al., 2019; Li et al., 2020).

$$\tau_{mix} = \frac{d_p^2}{4\pi^2 D_b} \quad (9)$$

$$D_b = D_c(\frac{\eta_c}{\eta})^\xi \quad (10)$$

in which ξ is an empirical fit parameter and we used 0.93 here, η_c is the crossover viscosity and we used 10^{-3} Pa s here. D_c is the crossover diffusion coefficient where the fractional Stokes-Einstein (Eq. (10)) and the Stokes-Einstein (Eq. (11)) predict the same diffusion coefficient (Evoy et al., 2019). In the Stokes-Einstein equation, k, and R_H are Boltzmann constant and diffusing radius respectively, T and η represent temperature and viscosity in ambient air.

$$D_c = \frac{kT}{6\pi\eta R_H} \quad (11)$$

2 Results

2.1 Inorganic nitrate and organic nitrate

During the calibration, the NO_x ratio (NO_2^+/NO^+) of standard ammonium nitrate particles (R_{NH4NO3}) was measured with an average result of 0.28 (Fig. S7a). The NO_2^+/NO^+ ratio of organic nitrate (R_{ONO2}) was estimated by dividing R_{NH4NO3} by a factor of 2.75 proposed by Day et al. (2022), thus the R_{ONO2} ratio in this study is 0.1. The fraction of organic nitrate and inorganic nitrate can be estimated based on the following equations (Farmer et al., 2010):

$$f_{\mathrm{RONO2}} = \frac{(R_{amb} - \mathrm{R_{NH4NO3}})(1+R_{\mathrm{ONO2}})}{(R_{\mathrm{ONO2}} - \mathrm{R_{NH4NO3}})(1+R_{amb})} \quad (12)$$

$$f_{\mathrm{RONO2}} = 1 \ \ (f_{\mathrm{RONO2}} > 1) \quad (13)$$

$$f_{\mathrm{NH4NO3}} = 1 - f_{\mathrm{RONO2}} \ \ (0 < f_{\mathrm{RONO2}} < 1) \quad (14)$$

$$f_{\mathrm{NH4NO3}} = 1 \ (f_{\mathrm{RONO2}} < 0) \quad (15)$$

References:

Canonaco, F., Crippa, M., Slowik, J. G., Baltensperger, U., and Prévôt, A. S. H.: SoFi, an IGOR-based interface for the efficient use of the generalized multilinear engine (ME-2) for the source apportionment: ME-2 application to aerosol mass spectrometer data, Atmospheric Measurement Techniques, 6, 3649-3661, 10.5194/amt-6-3649-2013, 2013.

Cappa, C. D. and Jimenez, J. L.: Quantitative estimates of the volatility of ambient organic aerosol, Atmospheric Chemistry and Physics, 10, 5409-5424, 10.5194/acp-10-5409-2010, 2010.

Cubison, M. J., Ortega, A. M., Hayes, P. L., Farmer, D. K., Day, D., Lechner, M. J., Brune, W. H., Apel, E., Diskin, G. S., Fisher, J. A., Fuelberg, H. E., Hecobian, A., Knapp, D. J., Mikoviny, T., Riemer, D., Sachse, G. W., Sessions, W., Weber, R. J., Weinheimer, A. J., Wisthaler, A., and Jimenez, J. L.: Effects of aging on organic aerosol from open biomass burning smoke in aircraft and laboratory studies, Atmospheric Chemistry and Physics, 11, 12049-12064, 10.5194/acp-11-12049-2011, 2011.

Day, D. A., Campuzano-Jost, P., Nault, B. A., Palm, B. B., Hu, W., Guo, H., Wooldridge, P. J., Cohen, R. C., Docherty, K. S., Huffman, J. A., de Sá, S. S., Martin, S. T., and Jimenez, J. L.: A Systematic Re-evaluation of Methods for Quantification of Bulk Particle-phase Organic Nitrates Using Real-time Aerosol Mass Spectrometry, Atmos. Meas. Tech. Discuss., 2021, 1-35, 10.5194/amt-2021-263, 2021.

Day, D. A., Campuzano-Jost, P., Nault, B. A., Palm, B. B., Hu, W., Guo, H., Wooldridge, P. J., Cohen, R. C., Docherty, K. S., Huffman, J. A., de Sá, S. S., Martin, S. T., and Jimenez, J. L.: A systematic re-evaluation of methods for quantification of bulk particle-phase organic nitrates using real-time aerosol mass spectrometry, Atmospheric Measurement Techniques, 15, 459-483, 10.5194/amt-15-459-2022, 2022.

DeRieux, W.-S. W., Li, Y., Lin, P., Laskin, J., Laskin, A., Bertram, A. K., Nizkorodov, S. A., and Shiraiwa, M.: Predicting the glass transition temperature and viscosity of secondary organic material using molecular composition, Atmospheric Chemistry and Physics, 18, 6331-6351, 10.5194/acp-18-6331-2018, 2018.

Dette, H. P., Qi, M., Schroder, D. C., Godt, A., and Koop, T.: Glass-forming properties of 3-methylbutane-1,2,3-tricarboxylic acid and its mixtures with water and pinonic acid, J Phys Chem A, 118, 7024-7033, 10.1021/jp505910w, 2014.

Emanuelsson, E. U., Watne, A. K., Lutz, A., Ljungstrom, E., and Hallquist, M.: Influence of humidity, temperature, and radicals on the formation and thermal properties of secondary organic aerosol (SOA) from ozonolysis of beta-pinene, J Phys Chem A, 117, 10346-10358, 10.1021/jp4010218, 2013.

Evoy, E., Maclean, A. M., Rovelli, G., Li, Y., Tsimpidi, A. P., Karydis, V. A., Kamal, S., Lelieveld, J., Shiraiwa, M., Reid, J. P., and Bertram, A. K.: Predictions of diffusion rates of large organic molecules in secondary organic aerosols using the Stokes–Einstein and fractional Stokes–Einstein relations, Atmospheric Chemistry and Physics, 19, 10073-10085, 10.5194/acp-19-10073-2019, 2019.

Farmer, D. K., Matsunaga, A., Docherty, K. S., Surratt, J. D., Seinfeld, J. H., Ziemann, P. J., and Jimenez, J. L.: Response of an aerosol mass spectrometer to organonitrates and organosulfates and implications for atmospheric chemistry, Proc Natl Acad Sci U S A, 107, 6670-6675, 10.1073/pnas.0912340107, 2010.

Faulhaber, A. E., Thomas, B. M., Jimenez, J. L., Jayne, J. T., Worsnop, D. R., and Ziemann, P. J.: Characterization of a thermodenuder-particle beam mass spectrometer system for the study of organic aerosol volatility and composition, Atmos. Meas. Tech., 2009.

Grieshop, A. P., Logue, J. M., Donahue, N. M., and Robinson, A. L.: Laboratory investigation of photochemical oxidation of organic aerosol from wood fires 1: measurement and simulation of organic aerosol evolution, Atmos. Chem. Phys., 9, 1263-1277, 10.5194/acp-9-1263-2009, 2009a.

Grieshop, A. P., Miracolo, M. A., Donahue, N. M., and Robinson, A. L.: Constraining the Volatility Distribution and Gas-Particle Partitioning of Combustion Aerosols Using Isothermal Dilution and Thermodenuder Measurements, Environmental Science & Technology, 43, 4750-4756, 10.1021/es8032378, 2009b.

Hu, W., Palm, B. B., Day, D. A., Campuzano-Jost, P., Krechmer, J. E., Peng, Z., de Sá, S. S., Martin, S. T., Alexander, M. L., Baumann, K., Hacker, L., Kiendler-Scharr, A., Koss, A. R., de Gouw, J. A., Goldstein, A. H., Seco, R., Sjostedt, S. J., Park, J.-H., Guenther, A. B., Kim, S., Canonaco, F., Prévôt, A. S. H., Brune, W. H., and Jimenez, J. L.: Volatility and lifetime against OH heterogeneous reaction of ambient
isoprene-epoxydiols-derived secondary organic aerosol (IEPOX-SOA), Atmospheric Chemistry and Physics, 16, 11563-11580, 10.5194/acp-16-11563-2016, 2016.

Hu, W. W., Hu, M., Yuan, B., Jimenez, J. L., Tang, Q., Peng, J. F., Hu, W., Shao, M., Wang, M., Zeng, L. M., Wu, Y. S., Gong, Z. H., Huang, X. F., and He, L. Y.: Insights on organic aerosol aging and the influence of coal combustion at a regional receptor site of central eastern China, Atmospheric Chemistry and Physics, 13, 10095-10112, 10.5194/acp-13-10095-2013, 2013.

Huang, R. J., Zhang, Y., Bozzetti, C., Ho, K. F., Cao, J. J., Han, Y., Daellenbach, K. R., Slowik, J. G., Platt, S. M., Canonaco, F., Zotter, P., Wolf, R., Pieber, S. M., Bruns, E. A., Crippa, M., Ciarelli, G., Piazzalunga, A., Schwikowski, M., Abbaszade, G., Schnelle-Kreis, J., Zimmermann, R., An, Z., Szidat, S., Baltensperger, U., El Haddad, I., and Prevot, A. S.: High secondary aerosol contribution to particulate pollution during haze events in China, Nature, 514, 218-222, 10.1038/nature13774, 2014.

Huffman, J. A., Ziemann, P. J., Jayne, J. T., Worsnop, D. R., and Jimenez, J. L.: Development and Characterization of a Fast-Stepping/Scanning Thermodenuder for Chemically-Resolved Aerosol Volatility Measurements, Aerosol Science and Technology, 42, 395-407, 10.1080/02786820802104981, 2008.

Kolesar, K. R., Chen, C., Johnson, D., and Cappa, C. D.: The influences of mass loading and rapid dilution of secondary organic aerosol on particle volatility, Atmospheric Chemistry and Physics, 15, 9327-9343, 10.5194/acp-15-9327-2015, 2015.

Koop, T., Bookhold, J., Shiraiwa, M., and Pöschl, U.: Glass transition and phase state of organic compounds: dependency on molecular properties and implications for secondary organic aerosols in the atmosphere, Physical Chemistry Chemical Physics, 13, 19238-19255, 10.1039/C1CP22617G, 2011.

Kuwata, M., Zorn, S. R., and Martin, S. T.: Using elemental ratios to predict the density of organic material composed of carbon, hydrogen, and oxygen, Environ Sci Technol, 46, 787-794, 10.1021/es202525q, 2012.

Li, X., Dallmann, T. R., May, A. A., Tkacik, D. S., Lambe, A. T., Jayne, J. T., Croteau, P. L., and Presto, A. A.: Gas-Particle Partitioning of Vehicle Emitted Primary Organic Aerosol Measured in a Traffic Tunnel, Environ Sci Technol, 50, 12146-12155, 10.1021/acs.est.6b01666, 2016.

Li, Y., Day, D. A., Stark, H., Jimenez, J. L., and Shiraiwa, M.: Predictions of the glass transition temperature and viscosity of organic aerosols from volatility distributions, Atmospheric Chemistry and Physics, 20, 8103-8122, 10.5194/acp-20-8103-2020, 2020.

Louvaris, E. E., Florou, K., Karnezi, E., Papanastasiou, D. K., Gkatzelis, G. I., and Pandis, S. N.: Volatility of source apportioned wintertime organic aerosol in the city of Athens, Atmospheric Environment, 158, 138-147, 10.1016/j.atmosenv.2017.03.042, 2017.

May, A. A., Presto, A. A., Hennigan, C. J., Nguyen, N. T., Gordon, T. D., and Robinson, A. L.: Gas-particle partitioning of primary organic aerosol emissions: (2) diesel vehicles, Environ Sci Technol, 47, 8288-8296, 10.1021/es400782j, 2013a.

May, A. A., Presto, A. A., Hennigan, C. J., Nguyen, N. T., Gordon, T. D., and Robinson, A. L.: Gas-particle partitioning of primary organic aerosol emissions: (1) Gasoline vehicle exhaust, Atmospheric Environment, 77, 128-139, 10.1016/j.atmosenv.2013.04.060, 2013b.

May, A. A., Levin, E. J. T., Hennigan, C. J., Riipinen, I., Lee, T., Collett, J. L., Jimenez, J. L., Kreidenweis, S. M., and Robinson, A. L.: Gas-particle partitioning of primary organic aerosol emissions: 3. Biomass burning, Journal of Geophysical Research: Atmospheres, 118, 11,327-311,338, 10.1002/jgrd.50828, 2013c.

Mei, F., Setyan, A., Zhang, Q., and Wang, J.: CCN activity of organic aerosols observed downwind of urban emissions during CARES, Atmospheric Chemistry and Physics, 13, 12155-12169, 10.5194/acp-13-12155-2013, 2013.

Ng, N. L., Canagaratna, M. R., Zhang, Q., Jimenez, J. L., Tian, J., Ulbrich, I. M., Kroll, J. H., Docherty, K. S., Chhabra, P. S., Bahreini, R., Murphy, S. M., Seinfeld, J. H., Hildebrandt, L., Donahue, N. M., DeCarlo, P. F., Lanz, V. A., Prévôt, A. S. H., Dinar,

E., Rudich, Y., and Worsnop, D. R.: Organic aerosol components observed in Northern Hemispheric datasets from Aerosol Mass Spectrometry, Atmospheric Chemistry and Physics, 10, 4625-4641, 10.5194/acp-10-4625-2010, 2010.

Paciga, A., Karnezi, E., Kostenidou, E., Hildebrandt, L., Psichoudaki, M., Engelhart, G. J., Lee, B.-H., Crippa, M., Prévôt, A. S. H., Baltensperger, U., and Pandis, S. N.: Volatility of organic aerosol and its components in the megacity of Paris, Atmospheric Chemistry and Physics, 16, 2013-2023, 10.5194/acp-16-2013-2016, 2016.

Sato, K., Fujitani, Y., Inomata, S., Morino, Y., Tanabe, K., Hikida, T., Shimono, A., Takami, A., Fushimi, A., Kondo, Y., Imamura, T., Tanimoto, H., and Sugata, S.: A study of volatility by composition, heating, and dilution measurements of secondary organic aerosol from 1,3,5-trimethylbenzene, Atmospheric Chemistry and Physics, 19, 14901-14915, 10.5194/acp-19-14901-2019, 2019.

Sato, K., Fujitani, Y., Inomata, S., Morino, Y., Tanabe, K., Ramasamy, S., Hikida, T., Shimono, A., Takami, A., Fushimi, A., Kondo, Y., Imamura, T., Tanimoto, H., and Sugata, S.: Studying volatility from composition, dilution, and heating measurements of secondary organic aerosols formed during α-pinene ozonolysis, Atmospheric Chemistry and Physics, 18, 5455-5466, 10.5194/acp-18-5455-2018, 2018.

Ulbrich, I. M., Canagaratna, M. R., Zhang, Q., Worsnop, D. R., and Jimenez, J. L.: Interpretation of organic components from Positive Matrix Factorization of aerosol mass spectrometric data, Atmos. Chem. Phys., 9, 2891-2918, 10.5194/acp-9-2891-2009, 2009.

Xu, W., Chen, C., Qiu, Y., Li, Y., Zhang, Z., Karnezi, E., Pandis, S. N., Xie, C., Li, Z., Sun, J., Ma, N., Xu, W., Fu, P., Wang, Z., Zhu, J., Worsnop, D. R., Ng, N. L., and Sun, Y.: Organic aerosol volatility and viscosity in the North China Plain: contrast between summer and winter, Atmospheric Chemistry and Physics, 21, 5463-5476, 10.5194/acp-21-5463-2021, 2021.

Ylisirniö, A., Buchholz, A., Mohr, C., Li, Z., Barreira, L., Lambe, A., Faiola, C., Kari, E., Yli-Juuti, T., Nizkorodov, S. A., Worsnop, D. R., Virtanen, A., and Schobesberger, S.: Composition and volatility of secondary organic aerosol (SOA) formed from oxidation of real tree emissions compared to simplified volatile organic compound (VOC) systems, Atmospheric Chemistry and Physics, 20, 5629-5644, 10.5194/acp-20-5629-2020, 2020.

Zhang, Q., Jimenez, J. L., Canagaratna, M. R., Ulbrich, I. M., Ng, N. L., Worsnop, D. R., and Sun, Y.: Understanding atmospheric organic aerosols via factor analysis of aerosol mass spectrometry: a review, Analytical and Bioanalytical Chemistry, 401, 3045-3067, 10.1007/s00216-011-5355-y, 2011.

Table S1. Introduction on instruments for VOC, criteria regular gases and black carbon (BC)

Species	Instruments	Mode	Time resolution
Volatile organic compounds (VOCs)	on-line GC-FID		1 hour
NOx	Chemiluminescence NO-NO_2-NO_x Analyzer	Thermo 42i	1 min
SO_2	Pulsed Fluorescence SO_2 Analyzer	Thermo 43i	1 min
CO	Trace Level Enhanced CO Analyzer	Thermo 48i	1 min
O_3	Ozone Monitor	Thermo 49i	1 min
BC	7-band Aethalometer	Magee AE31	5 min

Table S2. Summary of fractions of ELVOC, LVOC and S/IVOC of OA, the residence time (RT) of TD as well as the O:C of aerosols.

Anthropogenic	ELVOC	LVOC	S/IVOC	O:C	RT(s)	References
Beijing (winter)	0.12	0.21	0.67	0.34	10	(Xu et al., 2021)
Gucheng (winter)	0.1	0.25	0.65	0.4	10	(Xu et al., 2021)
Beijing (summer)	0.13	0.235	0.635	0.53	7.4	(Xu et al., 2021)
Mexico City (spring)	0.27	0.31	0.42	0.52	21.2	(Cappa and Jimenez, 2010)
Athens (winter)	0.3	0.33	0.37	0.32	28	(Louvaris et al., 2017)
Paris (summer)	0.25	0.38	0.37	0.49	50	(Paciga et al., 2016)
Paris (winter)	0.3	0.29	0.41		50	(Paciga et al., 2016)
Dongying (spring)	0.52	0.26	0.22	0.85	20.2	This study
Biogenic	ELVOC	LVOC	S/IVOC	O:C	RT(s)	References
United State (summer)	0.41	0.43	0.16	0.98	10-15	(Hu et al., 2016)
Amazon	0.52	0.37	0.11			(Hu et al., 2016)

Table S3. Summary of fractions of ELVOC, LVOC and S/IVOC of FFOA, the residence time (RT) of TD as well as the O:C of aerosols.

Ambient	ELVOC	LVOC	S/IVOC	O:C	RT(s)	References
Beijing HOA (summer)	0.14	0.11	0.75	0.17	7.4	(Xu et al., 2021)
Beijing FFOA (winter)	0.05	0.25	0.7	0.1	10	(Xu et al., 2021)
Gucheng HOA (winter)	0.09	0.23	0.68	0.12	10	(Xu et al., 2021)
Gucheng CCOA (winter)	0.1	0.28	0.62	0.18	10	(Xu et al., 2021)
Mexico City (spring)	0.13	0.27	0.6	0.2	21.2	(Xu et al., 2021)
Paris (winter)	0.11	0.29	0.6	0.1	50	(Paciga et al., 2016)
Paris (summer)	0.13	0.24	0.63	0.21	50	(Paciga et al., 2016)
Athens (winter)	0.3	0.42	0.28	0.1	28	(Louvaris et al., 2017)
Dongying (spring)	0.44	0.2	0.37	0.55	20.2	This study
Laboratory	ELVOC	LVOC	S/IVOC	O:C	RT(s)	References
Diesel POA	0	0.03	0.97		56	(May et al., 2013a)
Diesel	0	0.02	0.98		16	(Grieshop et al., 2009b)
Diesel	0	0.09	0.91		16	(Grieshop et al., 2009a)
Traffic tunnel POA	0	0.12	0.88		10.6	(Li et al., 2016)
Gasoline POA	0	0.27	0.73		56	(May et al., 2013b)

Table S4. Summary of fractions of ELVOC, LVOC and S/IVOC of BBOA, the residence time (RT) of TD as well as the O:C of aerosols.

Ambient	ELVOC	LVOC	S/IVOC	O:C	RT(s)	References
Gucheng (winter)	0	0.48	0.52	0.21	10	(Xu et al., 2021)
Mexico City (spring)	0.04	0.27	0.69	0.38	21.2	(Cappa and Jimenez, 2010)
Athens (winter)	0.09	0.39	0.52	0.27	28	(Louvaris et al., 2017)
Dongying (spring)	0.51	0.38	0.11	0.37	20.2	(Sato et al., 2018)
Paris (winter)	0.19	0.3	0.51	0.1	50	(Paciga et al., 2016)
Laboratory	ELVOC	LVOC	S/IVOC	O:C	RT(s)	References
Wood smoke	0	0.05	0.95		16	(Grieshop et al., 2009b)
Wood smoke	0	0	1		16	(Grieshop et al., 2009a)
BBOA	0	0.2	0.8		56	(May et al., 2013c)

Table S5. Summary of fractions of ELVOC, LVOC and S/IVOC of OOA, the residence time (RT) of TD as well as the O:C of aerosols.

Anthropogenic	ELVOC	LVOC	S/IVOC	O:C	RT(s)	References
Ambient						
Beijing OPOA (winter)	0	0.32	0.68	0.34	10	(Xu et al., 2021)
Gucheng SOA (winter)	0	0.31	0.69	0.63	10	(Xu et al., 2021)
Beijing LO-OOA (winter)	0	0.36	0.64	0.68	10	(Xu et al., 2021)
Beijing LO-OOA (summer)	0	0.27	0.73	0.76	7.4	(Xu et al., 2021)
Beijing MO-OOA (winter)	0	0.4	0.6	0.86	10	(Xu et al., 2021)
Beijing MO-OOA (summer)	0	0.38	0.62	1.3	7.4	(Xu et al., 2021)
Mexico City SV-OOA (spring)	0.16	0.40	0.43	0.66	21.2	(Cappa and Jimenez, 2010)
Paris OOA (summer)	0.3	0.25	0.45		50	(Paciga et al., 2016)
Paris OOA (winter)	0.3	0.25	0.45	1.12	50	(Paciga et al., 2016)
Athens OOA (winter)	0.42	0.29	0.29	0.5	28	(Louvaris et al., 2017)
Transported-OOA (spring)	0.69	0.19	0.12	1.02	20.2	This study
Background-OOA (spring)	0.56	0.22	0.22	1.1	20.2	This study
Mexico City LV-OOA (spring)	0.34	0.37	0.29	0.77	21.2	(Cappa and Jimenez, 2010)
Laboratory						
1,3,5-TMB+OH dry	0.01	0.1	0.88		13	(Sato et al., 2019)
1,3,5-TMB+OH dry (aging)	0.04	0.2	0.76		13	(Sato et al., 2019)
pentadecane-SOA	0.04	0.54	0.42	0.53	15	(Faulhaber et al., 2009)
Biogenic	ELVOC	LVOC	S/IVOC	O:C	RT(s)	References
Ambient						
IEPOX-SOA US	0.6	0.37	0.03	0.51	10-15	(Hu et al., 2016)
IEPOX-SOA Amazon	0.54	0.44	0.02	0.74	10-15	(Hu et al., 2016)
Laboratory						
a-Pinene Ozonolysis	0.005	0.14	0.85		13	(Sato et al., 2018)
a-Pinene Ozonolysis (dry)	0.005	0.18	0.82		13	(Sato et al., 2018)

a-pinene (low OHexp)	0.21	0.72	0.09		(Ylisirniö et al., 2020)

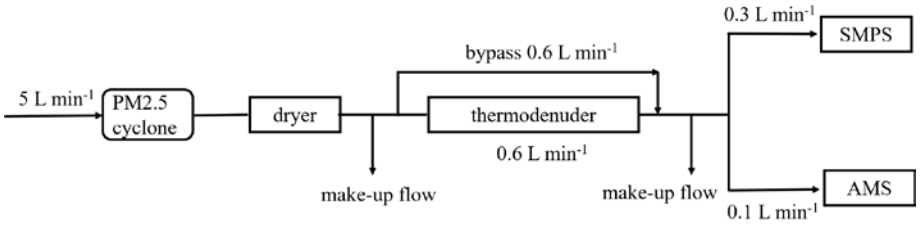

Figure S1. Brief schematic plot of sampling line in this campaign.

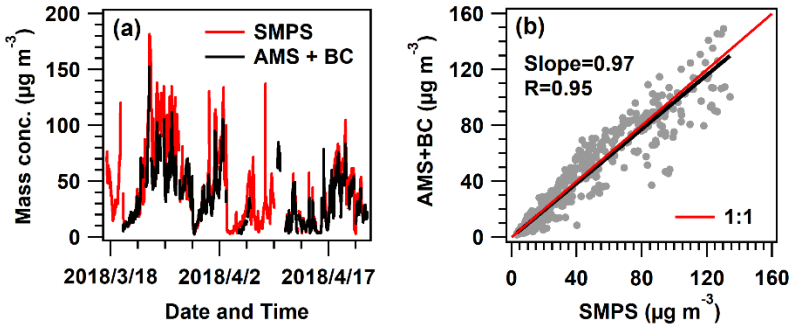

Figure S2. (a) Time series of total mass concentration of AMS (including equivalent BC from AE31) and SMPS in this campaign; (b) The scatter plot of calculated mass concentrations from AMS vs. mass from SMPS.

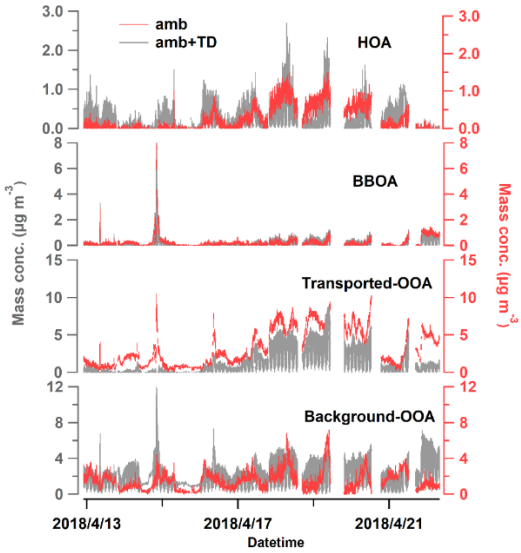

Figure S3 Comparison of OA factors variations between ambient (red) and ambient + TD (grey) resolved by ME-2 when constraining both HOA and BBOA and selecting 4 factors.

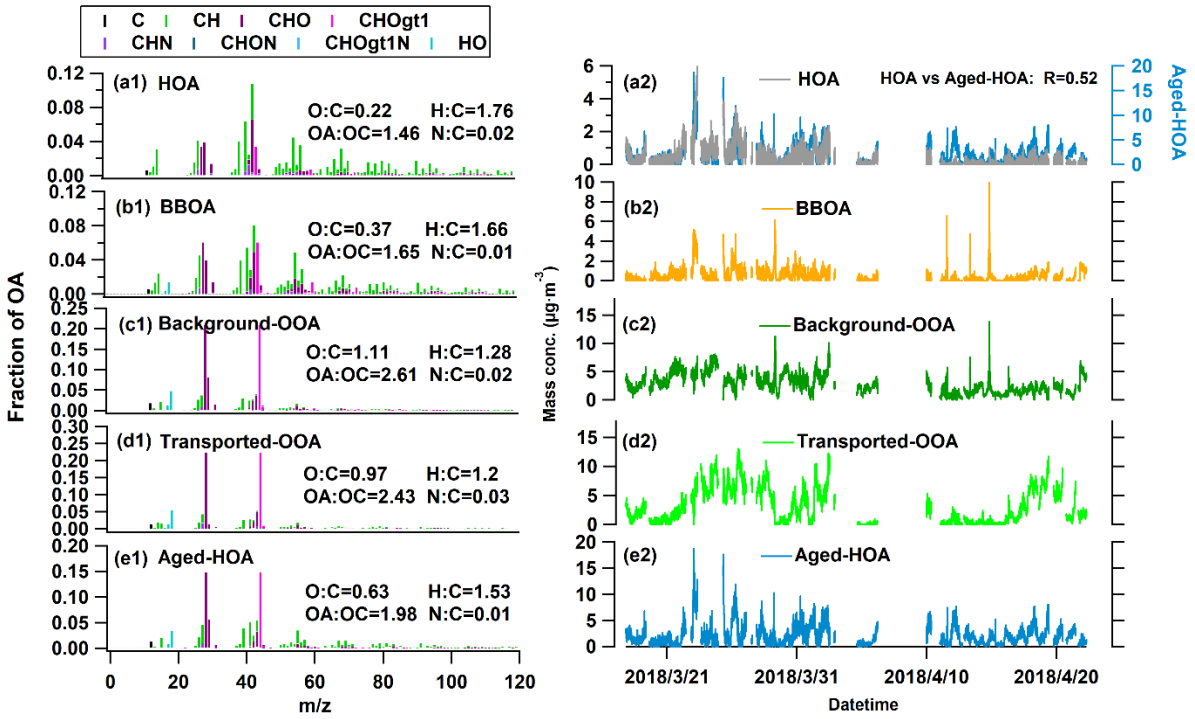

Figure S4. Spectrum and time series of 5 factors when constraining both HOA and BBOA. The constrained-HOA show good correlation with aged HOA

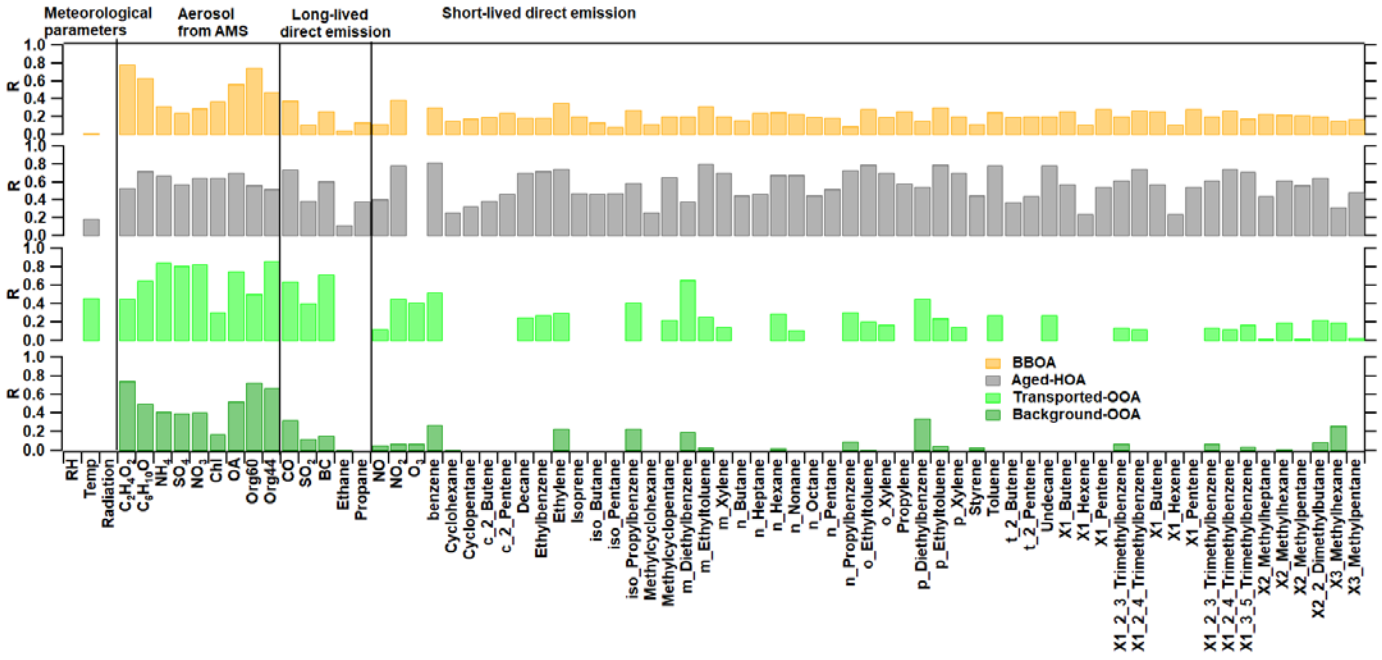

Figure S5. Pearson correlation coefficients for BBOA, aged HOA, transported-OOA and background-OOA versus species listed in x-axis. Negative values are not shown here.

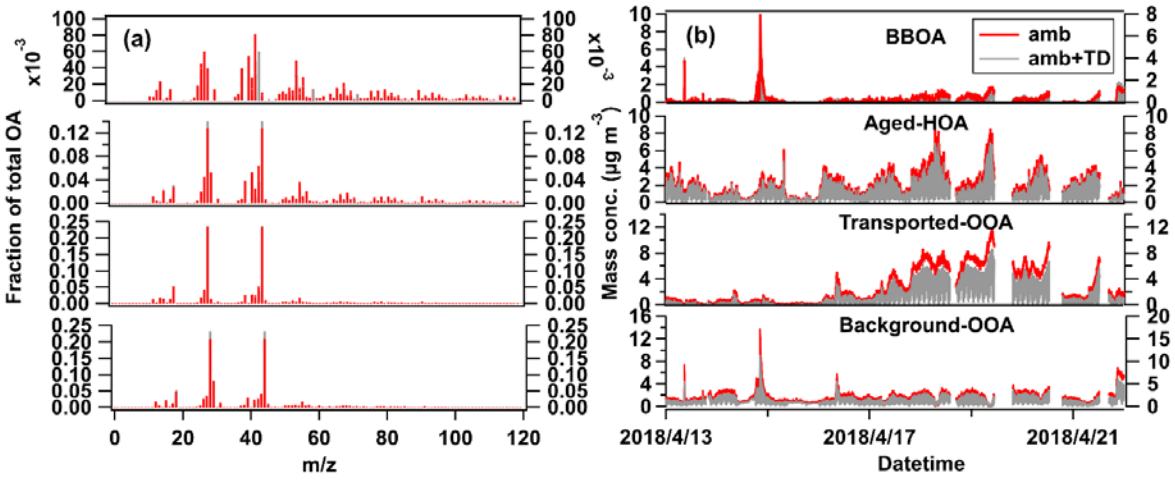

Figure S6. Comparison of OA factors and spectra between ambient (red) and ambient + TD (grey) resolved by ME-2.

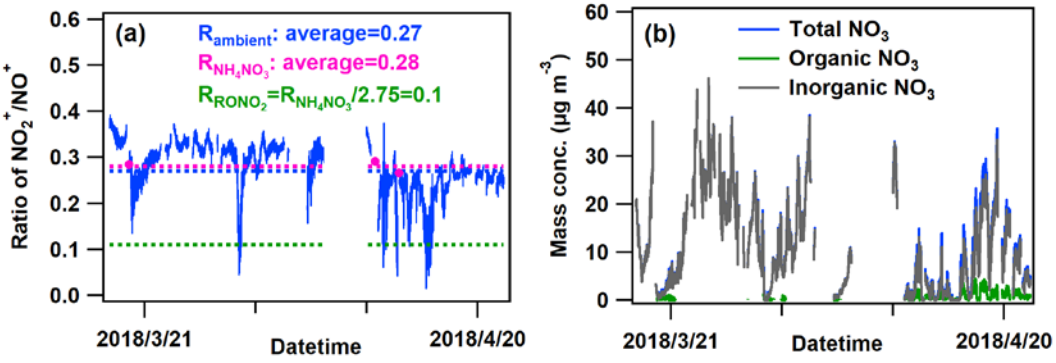

Figure S7. (a) Time series of the ratio of NO_2^+/NO^+ for ambient nitrate ($R_{ambient}$), pure ammonium nitrate (R_{NH4NO3}) and organic nitrate particles ($RONO_2$); (b) Time series of organic and inorganic nitrate based on the ratios of NO_2^+/NO^+ (Farmer et al., 2010; Day et al., 2021).

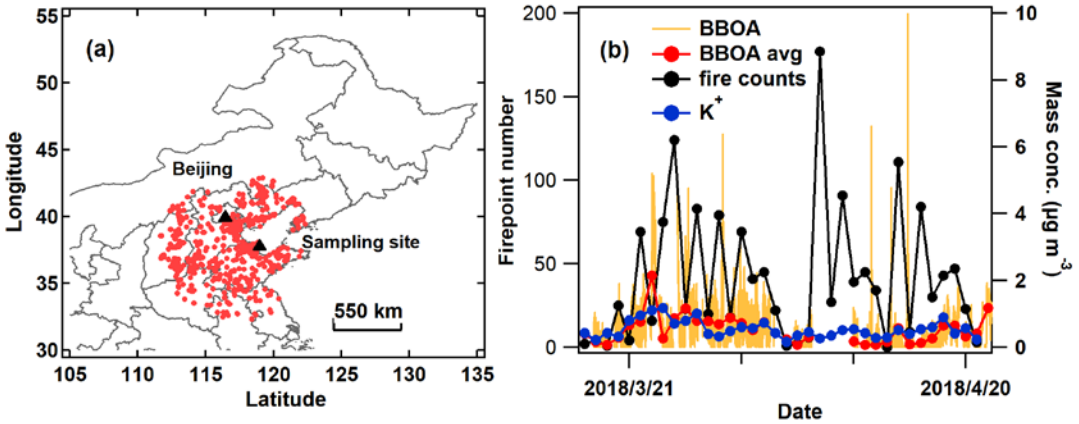

Figure S8. (a) Map of fire points in NCP during polluted period obtained by the Fire Information for Resource Management System (FIRMS) (https://firms.modaps.eosdis.nasa.gov/map); (b) Time series of fire points (left axis), mass concentrations of BBOA (per second and per day) and K^+.

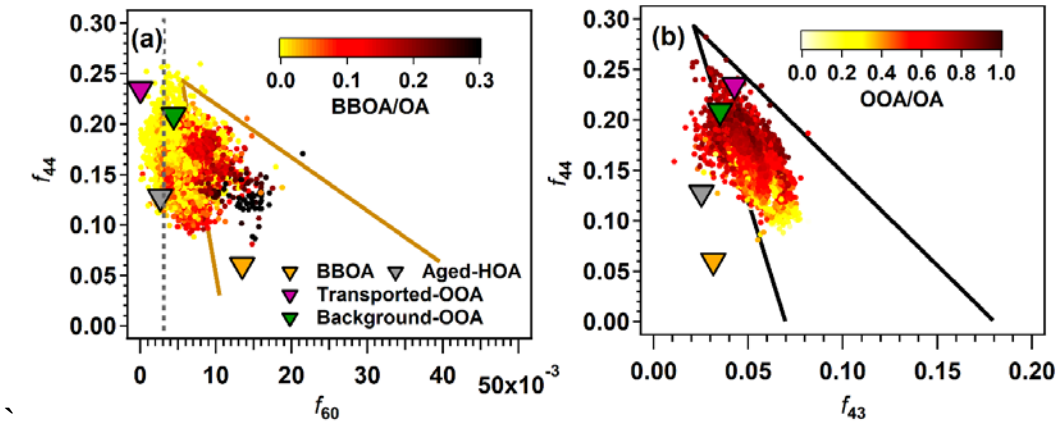

Figure S9. Scatter plots of (a) f_{44} vs f_{60} and (b) f_{44} vs f_{43}, color-coded by the fraction of BBOA and OOA respectively. According to Cubison et al. (2011), the brown triangle (a) is the biomass burning-influence area and the grey dashed line is the background value of f_{60} (=0.003) in non-biomass burning influenced areas. The black triangle in (b) represents OA oxidation area developed by Ng et al.(Ng et al., 2010).

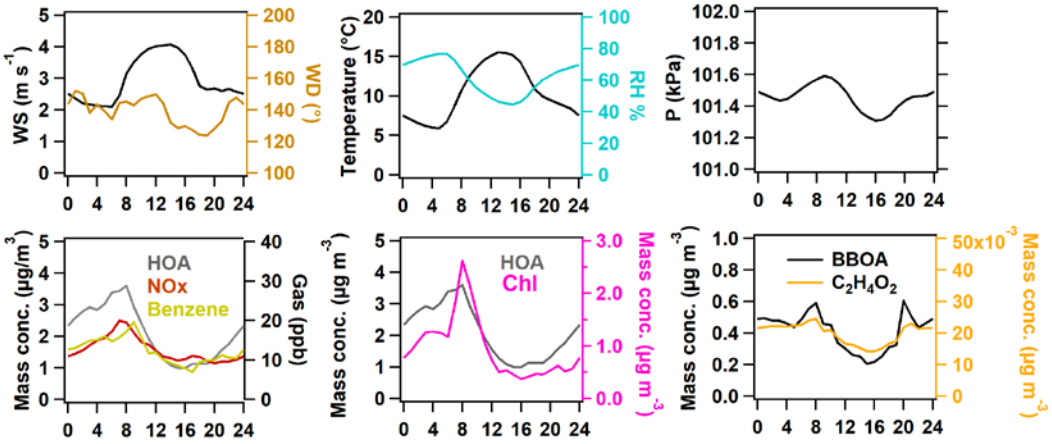

Figure S10. Average diurnal variations of meteorological parameters, OA factors and tracers in the entire study.

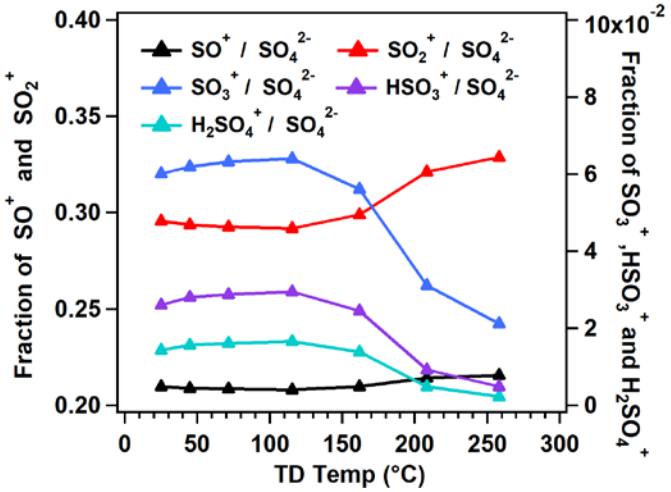

Figure S11. Variations in ratios of SO^+/SO_4^{2-}, SO_2^+/SO_4^{2-}, SO_3^+/SO_4^{2-}, HSO_3^+/SO_4^{2-}, $H_2SO_4^+/SO_4^{2-}$.